

Simulation of the coupled thermal/optical effects for liquid immersion nanolithography

So-Yeon Baek^a, Alexander Wei^b, Daniel C. Cole^a, Greg Nellis^b,
Michael S. Yeung^a, Amr Abdo^b, Roxann Engelstad^b, Mordechai Rothschild^c, and Michael Switkes^c

^aDept. Manufacturing Engineering, 15 St. Mary's St., Boston University, Boston, MA 02446, USA

^bComputational Mechanics Center, Department of Mechanical Engineering,
University of Wisconsin, Madison, WI 53706

^cLincoln Laboratory, Massachusetts Institute of Technology, 244 Wood Street,
Lexington, MA 02420, USA

ABSTRACT

Immersion lithography has been proposed as a method for improving optical microlithography resolution to 45 nm and below via the insertion of a high refractive index liquid between the final lens surface and the wafer. Because the liquid will act as a lens component during the imaging process, it must maintain a high, uniform optical quality. One potential source of optical degradation involves changes in the liquid's index of refraction caused by changing temperatures during the exposure process. Two-dimensional computational fluid dynamics models from previous studies have investigated the thermal and fluid effects of the exposure process on the liquid temperature associated with a single die exposure. Here, the global heating of the wafer from multiple die exposures has been included to better represent the "worst case" liquid heating that will

occur as an entire wafer is processed. The temperature distributions predicted by these simulations were used as the basis for rigorous optical models to predict effects on imaging. This paper presents the results for the fluid flow, thermal distribution, and imaging simulations. Both aligned and opposing flow directions were investigated for a range of inlet pressures that are consistent with either passive systems or active systems using filling jets.

Keywords: Optical lithography, liquid immersion, simulation, high NA

1. INTRODUCTION

The industry has spent a billion dollars or more on research to develop a next-generation lithography (NGL) technique capable of taking microelectronics fabrication to future nodes. Unfortunately, all of the competing NGL technologies are significantly different than the traditional optical methods used today and will therefore require an enormous investment in new infrastructure. Recently, there has been a revival of interest in a technique known as immersion lithography.¹⁻⁷ Immersion lithography attempts to increase the resolution and depth-of-focus of traditional optical lithography by replacing the air in the space between the lens and wafer with a liquid with a higher index of refraction, thereby increasing the effective numerical aperture (NA) of the system. By doing so, immersion microlithography appears capable of providing printability of critical dimensions (CDs) to below 65 nm using exposing radiation with a wavelength of $\lambda = 193$ nm. When liquid immersion is combined with other resolution enhancement techniques such as off-axis illumination and phase shift masks (PSM), still using $\lambda = 193$ nm, manufacturable CD printability below 50 nm appears achievable.⁸ Using $\lambda = 157$ nm would decrease these predictions yet further.⁸ In addition to impressive gains in resolution and depth-of-focus, the immersion lithographic technique is a popular option because it can be applied to current optical lithography processes with only relatively minor modifications, allowing much more of the existing infrastructure to be used when compared with other NGL techniques.

However, the introduction of the immersion liquid can lead to several potential issues, most of which revolve around either the fluidic and mechanical issues of adequately providing the liquid immersion region during the exposure stepping process from chip site to chip site, and/or the need for an extremely uniform liquid medium region, in terms of optical properties. Since the liquid

medium is to play a significant role in the optical imaging process, then concerns such as nonuniform fluid properties arising from a variety of possible sources, such as chemical leaching from the photoresist and microbubble formation, all need to be considered. A number of researchers have quite recently been intent on examining these potential problem areas, including: (1) the possible formation of air bubbles that may form when filling the air gap with liquid between the wafer and lens surface, (2) the normal and shear stresses induced on the lens via the presence of the flowing liquid, thereby possibly causing dynamic distortions and shifts in the lens mounting, and (3) nonuniform heating of the liquid during exposure, creating nonuniform index of refraction regimes that might also result in poor imaging properties. Reference 9 addressed aspects of issue (3) concerning the heating issues of the fluid under various fluid flow conditions and exposure stepping processes, while Ref. 8 discussed the impact on imaging due to changes in the liquid index of refraction properties. References 10, 11, and 12 addressed concerns about issues (1) and (2) using computational fluid dynamics (CFD) simulations.

The work described in Refs. 8 and 9 concerning issue (3) above, is continued in the present article, by taking the detailed heating effects simulated in Ref. 9, extending them somewhat, and then simulating the effects on optical imaging using the optical modeling method discussed in Ref. 8. In particular, Ref. 9 simulated the magnitude and distribution of the fluid temperature elevation associated with the exposure of a single chip on an otherwise unheated wafer. Here, this work is expanded to include the global heating of the wafer that occurs as multiple chips are exposed causing a gradual accumulation of energy in the wafer that manifests itself as an initial temperature rise prior to exposure in the later chips. Global simulations of the wafer exposure process have been developed and coupled to the single-die exposure model to predict the temperature distribution

associated with the “worst case” chip; i.e., the chip that is most severely preheated prior to exposure. Optical imaging methods have been developed that are capable of predicting the effect that the temperature induced changes in the fluid's index of refraction will have on the ultimate image that is developed on the photoresist.

Without question, there is an enormous number of factors that dictate whether the heating of the liquid immersion region will create imaging and printability problems for the very small structures that are desired to be printed with this technology. For starters, factors such as the fluid flow direction in the liquid immersion region, relative to wafer motion, the controlling pressures of the inlet and outlet fluid flows, as well as the shape of the jets, the thickness of the liquid immersion region, the radiation power incident on the exposure region, and the optical and thermal properties of the films and substrate, are all important parameters that will influence the results. The purpose of the simulation study presented here, as well as those in Refs. 8-12, is to bracket the more important of these properties and to examine and propose the more important engineering and physical changes that will be helpful to technologists developing immersion lithography tools. As a quick synopsis, it certainly seems that temperature shifts are controllable and containable, so as not to impose a roadblock on this exciting technology direction. However, as further pushes are made on controlling aberrations and printability, as inevitably will happen in the quest to extract as much as possible in terms of CD resolution and optimal process window conditions, then further control of some of the temperature variations predicted here may well be desired to be revisited.

As for the outline of this article, Section 2 describes the computational fluid dynamics models that were used to predict the temperature distribution in the immersion fluid. Section 3 describes the

optical model used to predict the imaging errors induced by the fluid heating. In Section 4, the results for a range of inlet pressures and two scanning configurations are presented, while the final section summarizes the results presented here and discusses possible future directions.

2. FLUID HEATING

In Fig. 1, a representative case of the simulation results associated with the semi-local exposure model presented by Wei et al.⁹ is shown. The configuration considered in Fig. 1 is an aligned configuration; the fluid is injected into the lens-wafer gap at the left-hand side of the picture (via a higher than ambient inlet pressure at this edge) and the wafer travels from left-to-right. Near the middle of the lens the fluid encounters the exposure region. Although the model is general enough to be applied to 157 nm lithography, the key parameters associated with the simulation shown in Fig. 1 have been set based on 193 nm anticipated conditions, summarized in Table 1. The absorption of incident exposure energy at 193 nm by the fluid is not large and the viscosity of water (the anticipated 193 nm immersion fluid) is low; therefore the fluid temperature near the lens and in the exposure region is not elevated significantly by absorption or viscous dissipation. The exposure energy passes through the fluid and is absorbed in the wafer, causing its temperature to rise. The fluid in contact with the wafer is subsequently heated, resulting in a thermally affected region that emanates from the exposure region and widens in the downstream direction.

Figure 1 shows the incoming wafer material (i.e., the silicon entering at the left hand side of the lens) at ambient temperature (assumed to be 300.00 K). This is consistent with exposing the first chip on a wafer. However, not all of the incident energy from the exposure laser is removed via the immersion liquid. Some of the energy remains in the wafer, and leaves the exposure area in the

form of elevated wafer temperatures which can be seen by the greater than ambient temperature of the wafer material at the right side of Fig. 1. The higher temperature portions of the wafer will then conduct heat to the cooler parts of the wafer, thereby causing as yet unexposed areas to undergo some temperature rise prior to being exposed.

A global finite element method has been developed to predict the transient temperature distribution across the entire wafer as it is exposed.⁹ The global model assumes that some percentage of the incident exposure energy is accumulated in the wafer; the remainder is removed by the fluid. The thermal loading associated with energy accumulation is applied as a moving, uniform heat flux that follows a serpentine scanning pattern. Figures 2(a-c) illustrate the temperature distribution across the wafer at various times during the exposure process for the case where 75% of the exposure energy is accumulated in the wafer material. Notice that the accumulated energy causes a temperature rise that extends a considerable distance away from the current exposure area into the surrounding wafer. The energy accumulated in the wafer is removed primarily via heat transfer to the chuck through a fairly large contact resistance and therefore this is a slow process; consequently, the temperature of the wafer on average rises during exposure.

Of primary interest here is the impact of this global temperature rise on the temperature distribution in the liquid within the lens-wafer gap. This effect results in preheated die regions prior to exposure. Figure 3 illustrates the predicted maximum and average temperature of the material in each die on the wafer immediately before it is exposed. In some dies, particularly those near the “turn-around” regions of the serpentine scanning pattern, the maximum temperature rise is over 0.1 K, and the average temperature rise for the die area is over 0.04 K. The magnitudes of these temperature rises

are significant relative to the fluid heating in the lens-wafer gap, as seen in the representative result shown in Fig. 1, where the maximum temperature rise is 0.16 K. The global model is used to correlate the maximum and average temperature rise predicted for the “worst-case” chip on the wafer as a function of the fraction of the incident energy accumulated in the wafer, shown in Fig. 4. Table 1 lists the important input parameters assumed for the global model.

The semi-local model allows the fraction of the incident energy accumulated in the under-lens region to be calculated. The temperature distribution in the lens-wafer gap for the “worst-case” chip is predicted by assuming that the wafer material enters the under-lens region with an elevated temperature that can be predicted using the global model according to Fig. 4. A schematic of the inputs and the resulting temperature profile for a representative case are shown in Fig. 5. In this case, it is seen that by increasing the wafer input temperature by 0.05 K, the maximum temperature rise of the liquid under the lens increases from 0.15 K to 0.18 K.

To determine an upper bound for the imaging errors, the heating simulations were run to steady state even though the exposure of a single die only requires 0.25 s. However, the thermal boundary conditions that best represent the situation are complex and a true prediction of the temperature distribution would require a full, wafer-level 3D simulation. The 2D steady state results aim to approximate the situation where the overall heating was most significant. To estimate the degree of conservatism associated with the steady-state temperature distribution, the integrated temperature rise was calculated by integrating the temperature elevation along the “worst-case optical path” (the right-hand side of the exposure region); this result is shown in Fig. 6 as a function of time. The integrated temperature rise is strongly correlated with the defocus error associated with the

temperature distribution. Notice that the integrated temperature rise will approach the steady-state results given sufficient time. Also notice that the steady-state temperature represents the largest temperature rise situation.

Figure 7 illustrates the steady-state temperature distribution predicted for the “worst-case” chip on the wafer in the aligned and opposing cases assuming a 200 Pa inlet pressure. Simulations were also carried out for both configurations for a range of other pressure conditions, as well as conditions involving some surprising outcomes regarding the transient versus steady state cases, as discussed more in Section 4.

3. ACCOUNTING FOR OPTICAL NONUNIFORMITIES IN LIQUID IMMERSION

REGION

Section 2 in Ref. 8 described the basic idea and underlying equations implemented for taking imaging distortions into account due to nonuniformities in the index of refraction within the liquid immersion region. The following section will briefly summarize and expand a bit upon the main physical idea, then turn to a detailed description of the specific exposure slit region modeled here.

The underlying physical mechanism for imaging distortions due to either thermal or material inhomogeneities in the liquid immersion region is that such changes can introduce changes in the real and imaginary parts of the liquid region as a function of position and time. Changes in the real part of the index of refraction will introduce changes in the optical path length of rays. If these distortions did not exist and the optical system was otherwise ideally designed, then a converging spherical wave in the image space would converge to a point at the Gaussian image plane.

However, with these distortions in the material properties of the medium in the image space, then phase changes would be introduced into the spherical wave, causing it to not perfectly converge to a point, and effectively introducing optical aberrations into the imaging system. Moreover, if the imaginary part of the index of the liquid medium is nonzero, and if this imaginary part varies as a function of position, then a spatially-dependent degradation in the amplitude of the radiation fields will be introduced. From a simulation perspective of calculating the aerial image of a mask, the difficulty involves incorporating the full 3D spatial changes in the index of refraction that might occur in the liquid regime, and accurately incorporating these effects on the electromagnetic fields as they propagate through this medium.

For all simulations carried out here, only changes in the real part of the index of refraction of the liquid medium were taken into account, as this is by far the main effect that is expected to occur for the purified water medium to be used in the 193 nm situations. To accomplish this task, changes in phase for rays traced to each point in the image plane were taken into account via the method discussed in Ref. 8. To examine the effects of liquid heating, first changes in temperature in fine divisions of space were calculated via the means discussed both here and in more detail in Ref. 9, then changes in phase of rays traversing through this region of space were calculated using interpolation means.

Undoubtedly at first glance, the very small temperature shifts in the liquid medium of only a fraction of a degree might seem utterly negligible in terms of introducing optical printing problems. However, it must be remembered that in this scenario the liquid has become a key part of the optical system; just as the inhomogeneities and surface deviations in highly refined lenses have always been

so tightly controlled; now these concerns become nearly as important for the liquid region. One might ask why these concerns have not been as significant a concern for the photoresist layer, where clearly thermal heating effects and material inhomogeneities have been present; the main reason is simply that the photoresist layer constitutes only a thickness of the order of $0.5\ \mu\text{m}$ or less, so small temperature differences in this much smaller region of material will introduce much smaller changes in optical path lengths, than might occur in the liquid immersion region, which is expected to be about 2000 times or more thicker than the photoresist region for the 193 nm situation.

Figure 8 shows a possible scheme for how the stepping process might proceed from chip to chip, as well as the scanning direction within each chip. The exposure slit indicated in Fig. 8 shows the region where light will illuminate the chip from the exposure system, with the slit scanning along the vertical direction of each chip, while steps are made horizontally from chip to chip along each row, then vertically from one row to the next. Four locations for fluid jets are indicated. Thus, in this scheme, it is easy to envision how fluid flow might occur either in the forward or reverse direction of the motion of the wafer with respect to the lens system. For the cases examined in Ref. 9, the temperature shifts in the liquid for fluid motion in the same direction as the wafer, are typically less than half the amount for when the fluid motion opposes the direction of wafer motion. Moreover, what clearly comes out of the work in Ref. 9 is that the faster the flow of liquid relative to the region of the chip to be exposed, then the less the temperature increase, as this scheme moves the heated liquid away from the region yet to be exposed. In the opposing fluid to wafer motion scenario, a far more complicated set of possibilities exist, as within the liquid medium, a reversal of flow can exist between the wafer and lens surface under a range of pressure conditions.

Figure 9 shows a cross section of the exposure slit, taken along the vertical direction in Fig. 8; the slit was assumed to be 5.0 mm in width. The temperature distribution as a function of position is again indicated, being a function of the fluid flow, due to the inlet pressure of the fluid and the precise design of the inlet and outlet jets. At each point in the slit, illumination rays from the exposure system are contained within the angular cone indicated in the diagram, dictated by the NA of the system. The optical program is able to take into account 3D changes in temperature in the fluid, although our thermal simulations to date have been confined to a vertical slice through the center of the exposure slit in Fig. 8, resulting in 2D distributions in temperature, as shown in Fig. 9.

4. PREDICTED EFFECT OF THERMAL NONUNIFORMITIES ON IMAGING

In this section we examine simulation predictions obtained for the imaging distortions due to liquid thermal heating effects under a variety of fluid flow conditions. The main methodology we followed was to place mask patterns of 65 nm dense lines and spaces (L/S) at various points within the 5.0 mm cross section of the exposure slit region shown in Fig. 9. Certainly more general conditions than lines and spaces could be examined, but, this seemed a reasonable starting point to ascertain the impact of these thermal variations. The typical results obtained are summarized in Fig. 10, which plots the contrast, $(I_{\max} - I_{\min}) / (I_{\max} + I_{\min})$, for these dense L/S patterns, for the thermal distribution shown in Fig. 9.

As can be seen, the effect of the thermal heating is largely to shift the contrast vs. focus plot by a constant, although different, amount for the three regions shown in the insert of Fig. 10. Undoubtedly the thermal inhomogeneities introduce other imaging aberrations than simply a focus shift. However, the predicted temperature change is not huge, and the predicted focus shift is

likewise not large. Since the contrast vs. focus plot essentially remains the same shape, other than a shift in focus, then we conclude that the other imaging aberrations (spherical, coma, etc.) resulting from the heating are yet smaller contributions to the imaging distortion than the focus change itself.

Figures 11-13 examine various situations of aligned and opposed fluid flow conditions, under a range of inlet pressure conditions from 0 to 2000 Pa. In addition, three mask/illumination conditions were examined for each of these inlet pressure conditions, namely: (1) the case of a binary mask, indicated by “Conventional”, with only clear and opaque regions present on the mask, with a circular partial coherence parameter of 0.6; (2) the case of a binary mask, but illuminated using annular illumination, indicated by “Annular,” with the inner and outer circular partial coherence parameters equal to 0.4 and 0.6, respectively; and (3) an alternating phase shift mask (alt PSM), with a circular partial coherence parameter equal to 0.3. The change in focus is plotted for each of these conditions.

Figure 11 shows the computed focus variation across the exposure beam under a variety of conditions. Here, the results for the exposure of the first and the 43rd chip of one wafer were included. The first chip represents the “coldest chip,” since exposure of the chips on the wafer would have just begun, while the 43rd chip represents the “hottest chip,” as this chip was predicted to be at the net highest average temperature as compared with all other chips, due to the particular stepping process and wafer layout assumed in the simulation. In addition, there are two other conditions contained in Fig. 11, namely, the “transient” and “steady-state” exposure cases. The transient 0.25 s exposure case here represents the time when the exposure scanning beam arrives at the end of a single-die exposure process. The steady-state is defined such that if the scan lasted not

just 0.25 s, but continued on indefinitely, then the temperature rise at all points in the exposure slit would approach a constant amount per point, although not the same amount from one point to the next. This “steady-state” case seemed of interest, as possibly constituting a “worst-case” scenario. However, of course this concept is not really physically realistic since one cannot physically obtain an infinite time in exposure while scanning, since the scan would run past the dimension of one chip, and later off the edge of the wafer! Still, the concept seemed useful as a comparison tool since one can well imagine an infinitely sized wafer, where one continues to scan at a constant rate indefinitely.

Surprisingly, the transient 0.25 s exposure case had a slightly larger focus variation across the slit than the steady-state case, except for the 0 Pa of inlet pressure situation at the 43rd chip. This result was initially unexpected because intuitively it seemed obvious that the steady-state case would exhibit the larger optical change due to the higher temperature rise expected. However, even though the steady-state situation resulted in higher net temperatures, the temperature distribution at points of both edges of the exposure slit was also slightly more “uniform” in the steady-state case than in the 0.25 s transient case. This less uniform temperature distribution in the 0.25 sec transient case actually made this situation a more “worst-case” situation than the higher, but more uniform temperature distribution in the steady-state case. As for the other somewhat contradictory case of the situation with the 0 Pa of inlet pressure, here there was no fluid flow. Therefore, the steady-state simulation case at the 43rd chip resulted in the highest temperature distribution obtained because of the pre-exposure temperature rise on the wafer, thereby causing a larger focus shift as compared to the case of exposure for the first chip.

Regardless of the transient 0.25 s exposure case versus the steady-state case, or the chip numbers that indicates a location on the wafer, the trend and amount of the change in focus are very similar. For this reason, the transient 0.25s exposure case data will be used for subsequent discussion and analysis, unless noted otherwise.

Several other general conclusions can be immediately seen from Fig. 11. First, generally, the higher the inlet pressure, the smaller the change in focus shift across the exposure slit. This statement holds for both the aligned and opposed fluid flow directions. Roughly speaking, this effect should be somewhat expected, since as the inlet pressure increases, the fluid flow becomes faster, thereby helping to reduce the temperature gradient across the slit.

Second, at lower inlet pressures, the change in focus across the slit is substantially smaller for the aligned flow versus the opposed flow situations, although at higher inlet pressure conditions, the opposed fluid flow situation actually introduces a smaller focus change across the slit than for the aligned fluid flow case. Presumably this situation arises because of the complicated thermal distribution that occurs within the liquid region between the lens and the wafer, which in some cases may be higher nearer the wafer, but then might also diminish more rapidly away from the wafer due to the complex fluid flow that can arise.

Other points that can be noted from Fig. 11 are that, for the line/space pattern examined, and for the particular annular versus PSM situation examined, the PSM method was more effective in reducing thermally induced focus shifts than the annular illumination technique. Moreover, it should be emphasized that the change in focus shift across the exposure slit is considerably smaller than the

absolute focus shift that would occur in the thermal versus “no-heated” situation shown in Fig. 10. Comparing Fig. 11 to Fig. 12 clearly makes this point as well.

Finally, the most important conclusion from this analysis is that the change in focus is predicted to be about 1 nm or less for both the aligned and opposed fluid flow situations when the inlet pressure is above 200 Pa, and even smaller (i.e., below a negligible amount of 0.2 nm) when the inlet pressure is above 750 Pa. This result certainly enormously alleviates the concerns of this heating effect for the $\lambda=193$ nm liquid immersion case using water. Even if the simulation did not fully adequately capture aspects of the liquid immersion technology when put into practice, such as different jet configurations, etc., still, this very small change is indicative of considerable room for flexibility.

Figure 12 examined how much the focus at the center of the slit is predicted to shift during the scans of the first and the 43rd chips. As should be expected, the focus changes in Fig. 12 are much larger than the sub 0.2 nm focus shifts across the exposure slit that appear readily achievable in either aligned or opposed fluid flow conditions in Figs. 11, provided high enough inlet pressures are utilized. Figure 12 thus provides insight into how the incorporation of automated predictive focus sensors and controls would aid to minimize this “across chip” focus shift due to thermal effects.

Figure 13 examined the focus shift at the center of the exposure slit due to thermal effects predicted to occur across the wafer. Here the focus variation was computed between the initial stage and the most heated spot on the wafer. Figure 13(a) was found to be similar to the “across chip” focus variation at the most heated chip (43rd chip) [i.e., Fig. 12(b)], since the most heated spot was on the

43rd chip at the 0.25 s point of scan time, and the temperature distribution for the start of the scan on the 43rd chip was similar to the start of the scan on the first chip, with only pre-exposure heat (from previous scans at neighboring chips) distinguishing the situations.

While Fig. 13(a) examined the expected more realistic transient results, Fig. 13(b) examined the “across wafer” focus shifts if the steady-state exposure model was employed. As can be seen, the focus shift at the center of the exposure slit is certainly predicted to be much larger here, thereby providing a nice “worst case” scenario for the focus shift of the center of the slit across the wafer due to these thermal effects. It is most interesting to note again, however, that the more important concern of the focus change across the slit is smaller for the steady-state model than for the physically more realistic transient model [Fig. 11]. Again, the reason for this subtle effect is that the steady-state situation certainly increases the average temperature of the liquid in the exposure slit region, but the transient case exhibited a larger temperature gradient across the same region.

Examining Figs. 11-13 reveals that instead of absolute focus shift up to 7 nm or more being the real concern, the main points should be the focus shift within the exposure slit region, and the focus shifts that occur when completely scanning one chip region. As the scan of one chip occurs, the heating effects change, resulting in imaging changes. Fortunately, the latter concern of the focus shift within the scan of one chip, should be capable of being reduced significantly via perhaps a combination of (1) measuring and physically changing defocus conditions during the scan, and (2) aiding such determinations by using an algorithm to anticipate such changes due to heating and to thereby act as a starting point for feedback control.

5. CONCLUDING REMARKS

A broad range of conditions have been examined here for 193 nm projection microlithography, assuming a liquid immersion region between the last lens and the wafer, with a thickness of 1.0 mm. Conditions with fluid flow both in the same direction as well as opposed to the wafer and scanning directions, were considered. A “global” heating effect was included in the present work, meaning, that as each die is scanned, the neighboring die regions will also heat up, thereby resulting in a different heating effect for each die, based on its location in the wafer, and on the past stepping and scanning history of previous dies on the wafer.

These heating effects were taken into account via rigorous optical modeling methods pursued here. Conditions of binary mask, annular illumination, and PSM were examined. The main consequence of the heating of the liquid was an effective focus shift in the imaging of structures. Undoubtedly the heating also introduces other imaging aberrations, but the focus shift was found to be the most significant. The net focus changes between “no heating” and “heating” were of the order of several nanometers, but, the more significant result was the change in focus from one position to another along the exposure slit, and along the scan direction. The change in focus along the scan should readily be controllable, via using automated focusing changes, perhaps combined with an algorithm for predicting heating effects and consequent focus shifts. The change in focus across the exposure slit cannot be addressed in the same way. However, as shown here, by using sufficiently high inlet pressure conditions, to ensure more rapid flow and consequently lower accumulated heating effects, this change in focus across the slit appears containable for the anticipated 193 nm liquid immersion exposure systems.

ACKNOWLEDGMENTS

This work has been supported by DARPA/ARL, the Semiconductor Research Corporation (SRC), and International SEMATECH. Computer support was provided by the Intel Corporation and Microsoft. We also thank Dr. W. Trybula for his close interaction and support during the course of this work.

REFERENCES

1. M. Switkes and M. Rothschild, "Resolution Enhancement of 157 nm Lithography by Liquid Immersion," *J. Microlith., Microfab., Microsyst.*, Vol. 1, No. 3, pp. 225-228, 2002.
2. M. Switkes, M. Rothschild, "Immersion Lithography at 157 nm," *J. Vac. Sci. Technol. B*, Vol. 19, No. 6, pp. 2353-2356, 2001.
3. B. J. Lin, "The Future of Subhalf-Micrometer Optical Lithography," *Microelectron. Eng.*, Vol. 6, pp. 31-51, 1987.
4. K. Takahashi, "Immersion Type Projection Exposure Apparatus," United States Patent 5610683, 1997.
5. W. W. Tabarelli, "Verfahren und Vorrichtung zum Kopieren eines Musters auf eine Halbleiterscheibe," European Patent EP23231, 1981.
6. T. A. Brunner, N. Seong, W. D. Hinsberg, J. A. Hoffnagle, F. A. Houle, and M. I. Sanchez, "High NA Lithography Imagery at Brewster's Angle," *Proc. SPIE*, Vol. 4691, pp. 1-10, 2002.
7. B. W. Smith and J. Cashmore, "Challenges in High NA, Polarizations, and Photoresists," *Proc. SPIE*, Vol. 4691, pp. 11-24, 2002.
8. S.-Y. Baek, D. C. Cole, M. Rothschild, M. Switkes, and E. Barouch, "Simulation Study of Process Latitude for Liquid Immersion Lithography," *Journal of Microlithography, Microfabrication, and Microsystems*, Vol. 3 (01), pp. 52-60 (2004).
9. A. Wei, A. Abdo, G. Nellis, R. Engelstad, J. Chang, E. Lovell, and W. Beckman, "Simulating Fluid Flow Characteristics During the Scanning Process for Immersion Lithography," *J. Vac. Sci. Technol. B*, Vol. 21, No. 6, pp. 2788-2793, 2003.

10. A. Wei, A. Abdo, G. Nellis, R. Engelstad, J. Chang, E. Lovell, and W. Beckman, "Modelling Fluid Thermomechanical Response for Immersion Lithography Scanning," *Microelectron. Eng.*, 2004 (in press).
11. A. Wei, G. Nellis, A. Abdo, R. Engelstad, J. Chang, M. Switkes, and M. Rothschild, "Preliminary Microfluidic Simulation for Immersion Lithography," *Proc. SPIE*, Vol. 5040, 2003.
12. A. Wei, G. Dicks, A. Abdo, G. Nellis, R. Engelstad, J. Chang, E. Lovell, and W. Beckman, "Predicting Microfluidic Response During Immersion Lithography Scanning," *Proc. 20th European Mask Conference on Mask Technology for Integrated Circuits and Micro-Components*, VDE, Vol. 43, 2004.

Material Properties				
	Water	Photoresist	SiO ₂	Silicon Wafer
Thickness	1.0 mm	150 nm	1.0 μm	625 μm
Thermal Conductivity (W/m-K)	0.6	0.2	1.4	168
Specific Heat (J/kg-K)	4180	1500	1000	750
Density (kg/m ³)	1000	1200	2270	2330
Semi-Local Wafer Movement (m/s)	0.16			
Input Parameters				
Contact Conductance	150 W/m ² -K			
Gap Height	1.0 mm			
Lens Length	100.0 mm			
Illumination Beam Width	5.0 mm			
Power on Wafer	611.0 mW/cm ²			
Fields per wafer	71			
Field size at wafer (4 : 1 reduction)	25 mm × 32 mm			
Illumination field width	5.0 mm			
Scan velocity	160 mm/s			
Scan time per field	0.231 s			
Stage stepping time per field	0.112 s			
Resist sensitivity	20 mJ/cm ²			
Equivalent heat flux	155.0 mW/cm ²			

Table 1. Material and input parameters for the heating models.

FIGURE CAPTIONS

Fig. 1: Representative thermal profile in the wafer and the fluid in the lens-wafer gap for the first chip exposure process.⁹

Fig. 2: Temperature contours over the wafer for the particular case where 75% of the incident exposure energy is accumulated in the wafer after: (a) the 3rd exposure field, (b) the 36th exposure field, and (c) the 72nd exposure field.⁹

Fig. 3: Average and maximum temperatures in each die immediately before exposure predicted by the global model for the particular case where 75% of exposure energy is accumulated in the wafer.⁹

Fig. 4: Predictions of the maximum and average temperature rise for the “worst-case” chip on the wafer as a function of the fraction of the incident energy accumulated in the wafer.

Fig. 5: Representative temperature distribution in the lens-wafer gap during the exposure of the “worst-case” chip on the wafer. Note the elevated wafer inlet temperature.⁹

Fig. 6: The integrated temperature rise along the worst case optical path (which correlates with the defocus error) as a function of time for a representative “worst-case” chip exposure process. Notice that the integrated temperature rise approaches the steady-state value, which is conservative relative to the value at the end of a single-die exposure process (0.25 s).

Fig. 7: Steady-state temperature distribution predicted for the "worst-case" chip assuming a 200 Pa inlet pressure in the (a) aligned and (b) opposing configurations.

Fig. 8: A specific example depicting how the stepping and scanning process might proceed, with fluid flow arising from one or more of the four fluid jets shown.

Fig. 9: Vertical cross section of the exposure slit region in Fig. 8. The temperature distribution is indicated, along with the angular range of rays that are incident at each point.

Fig. 10: Contrast vs. focus for 65 nm L/S patterns placed at the left, center, and right edges of the 5.0 mm exposure slit region shown in Fig. 9. The insert to the right shows that each of these three conditions largely result in focus shifts of different amounts from the "no-heated" liquid condition.

Fig. 11: Focus variation across the slit, meaning, the difference in focus shifts between the left and right sides of the exposure slit. The solid lines indicate the case of aligned fluid flow while the dashed lines represent the opposed fluid flow case. Figs. 11(a) and 11(b) were examined at the point of 0.25 s of scanning (i.e., "transient case"), with Fig. 11(a) being the results for the 1st chip, and Fig. 11(b) being the results for the 43rd chip. Figs. 11(c) and 11(d) represent the results in the steady state scanning situation, with Fig. 11(c) being the results for the 1st and Fig. 11(d) being the results for the 43rd chip. The "1st chip" means the first scanning chip

of the wafer and the 43rd chip is the “hottest chip” in the wafer during the whole exposure process, for the particular scanning/stepping simulation case examined here.

Fig. 12: Focus variation across chips under different fluid flow conditions, as computed at the center of the exposure slit. Transient exposure times were examined between the 0.01 sec and 0.25 sec scan times. Fig. 12(a) pertains to the first chip, while Fig. 12(b) pertains to the 43rd chip.

Fig. 13: Focus variation across wafer under different fluid flow conditions, as computed at the center of the exposure slit. (a) Focus variation across wafer at transient 0.25 s exposure scan time. (b) Focus variation across wafer for the “steady-state” exposure model.

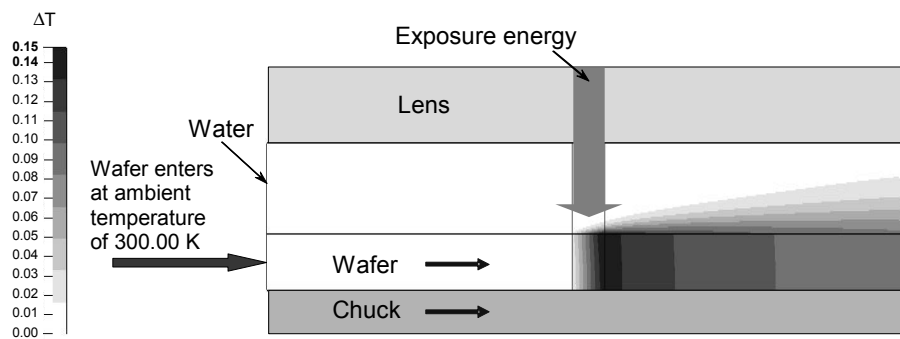


Fig. 1: Representative thermal profile in the wafer and the fluid in the lens-wafer gap for the first chip exposure process.⁹

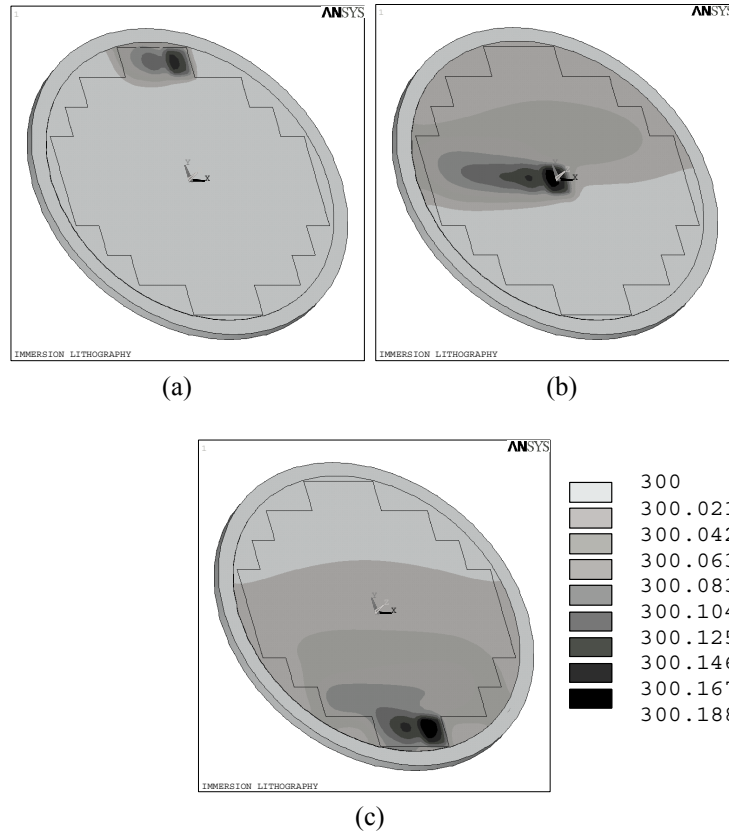


Fig. 2: Temperature contours over the wafer for the particular case where 75% of the incident exposure energy is accumulated in the wafer after: (a) the 3rd exposure field, (b) the 36th exposure field, and (c) the 72nd exposure field.⁹

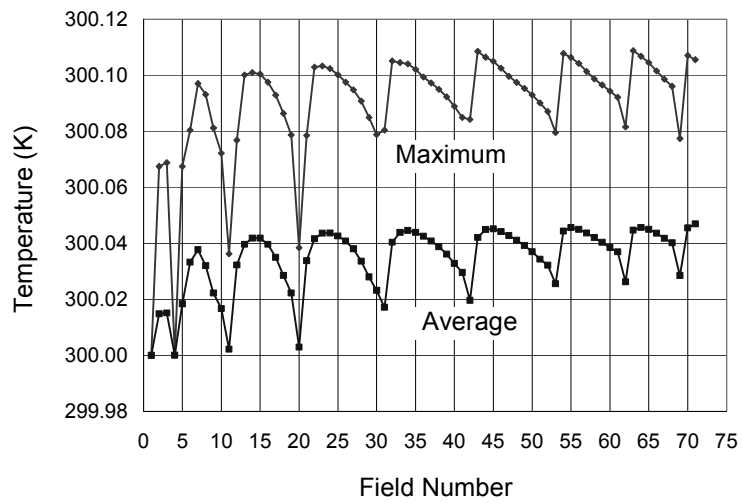


Fig. 3: Average and maximum temperatures in each die immediately before exposure predicted by the global model for the particular case where 75% of exposure energy is accumulated in the wafer.⁹

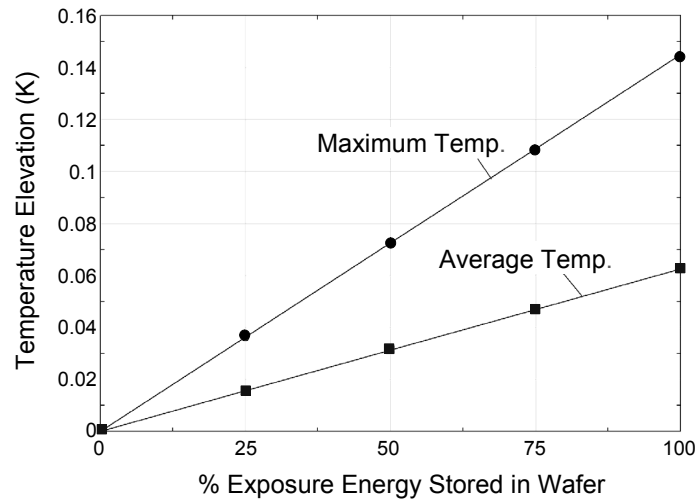


Fig. 4: Predictions of the maximum and average temperature rise for the “worst-case” chip on the wafer as a function of the fraction of the incident energy accumulated in the wafer.

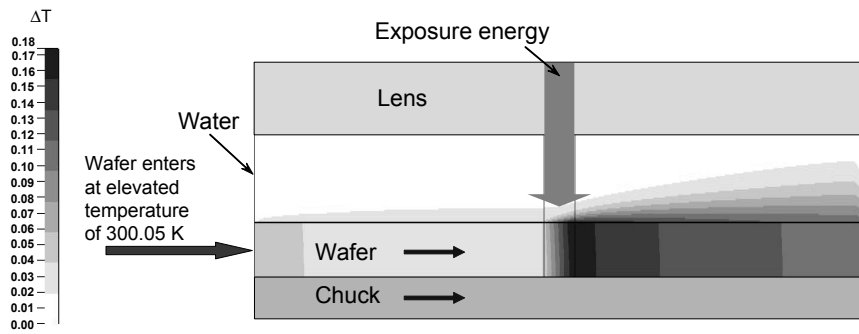


Fig. 5: Representative temperature distribution in the lens-wafer gap during the exposure of the “worst-case” chip on the wafer. Note the elevated wafer inlet temperature.⁹

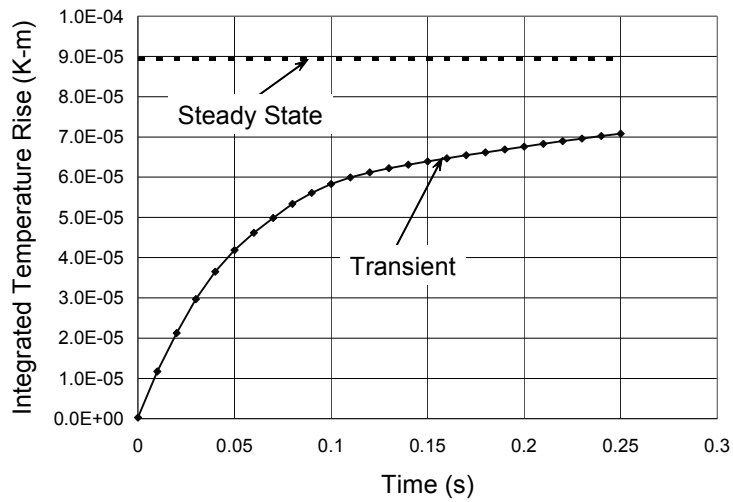


Fig. 6: The integrated temperature rise along the worst case optical path (which correlates with the defocus error) as a function of time for a representative “worst-case” chip exposure process. Notice that the integrated temperature rise approaches the steady-state value, which is conservative relative to the value at the end of a single-die exposure process (0.25 s).

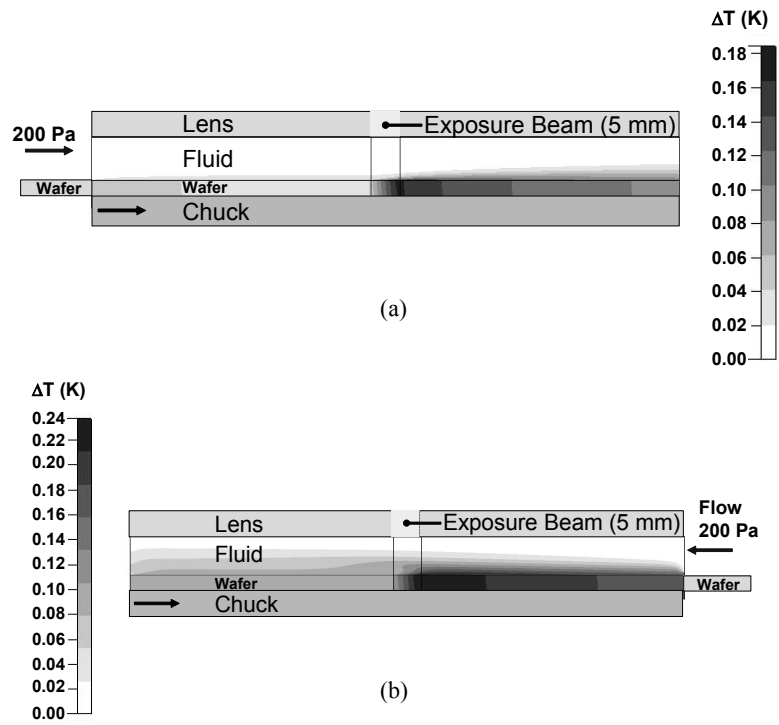


Fig. 7: Steady-state temperature distribution predicted for the "worst-case" chip assuming a 200 Pa inlet pressure in the (a) aligned and (b) opposing configurations.

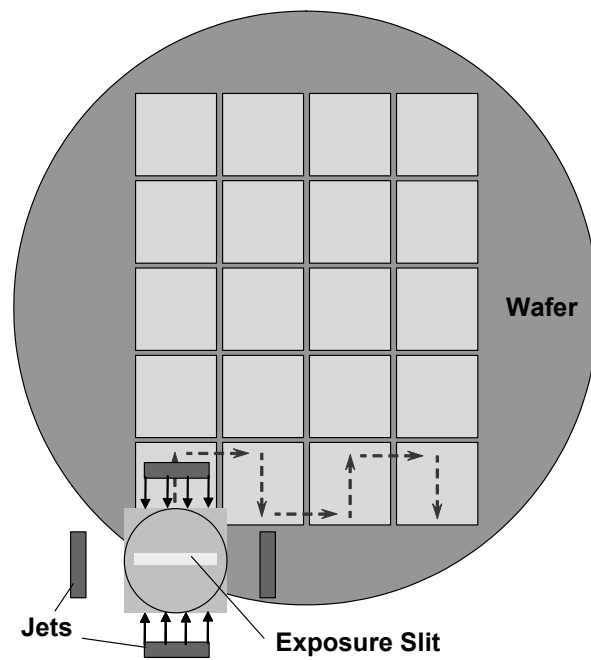


Fig. 8: A specific example depicting how the stepping and scanning process might proceed, with fluid flow arising from one or more of the four fluid jets shown.

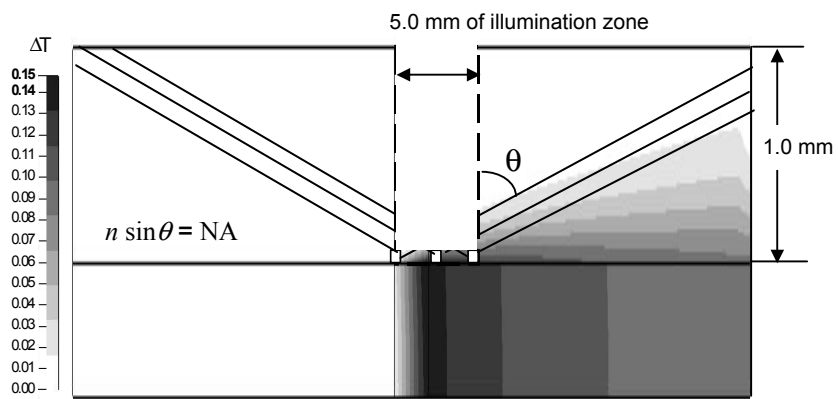


Fig. 9: Vertical cross section of the exposure slit region in Fig. 8. The temperature distribution is indicated, along with the angular range of rays that are incident at each point.

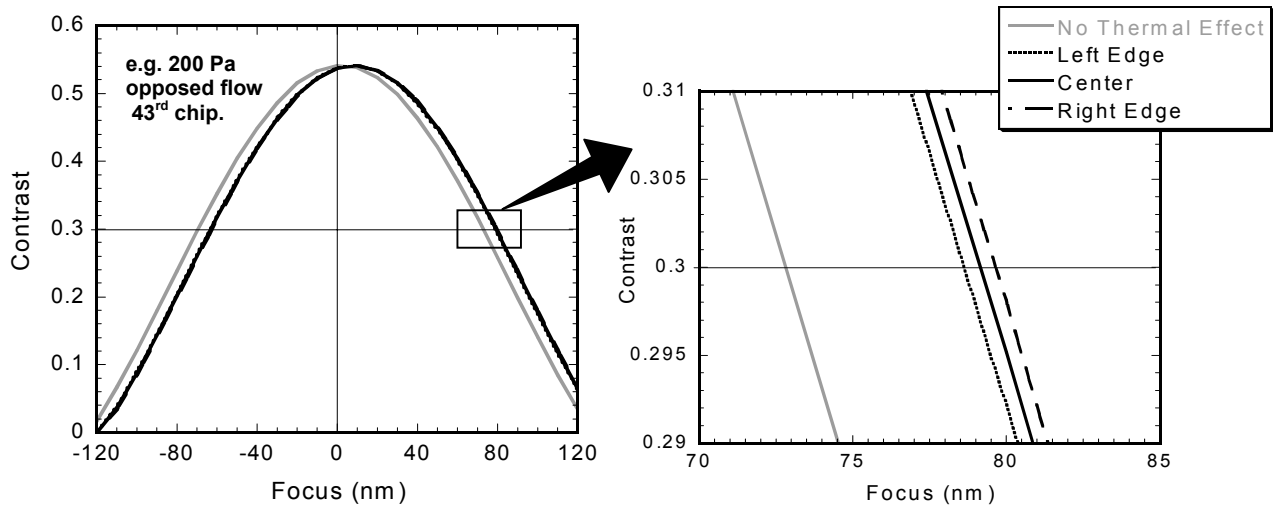


Fig. 10: Contrast vs. focus for 65 nm L/S patterns placed at the left, center, and right edges of the 5.0 mm exposure slit region shown in Fig. 9. The insert to the right shows that each of these three conditions largely result in focus shifts of different amounts from the “no-heated” liquid condition.

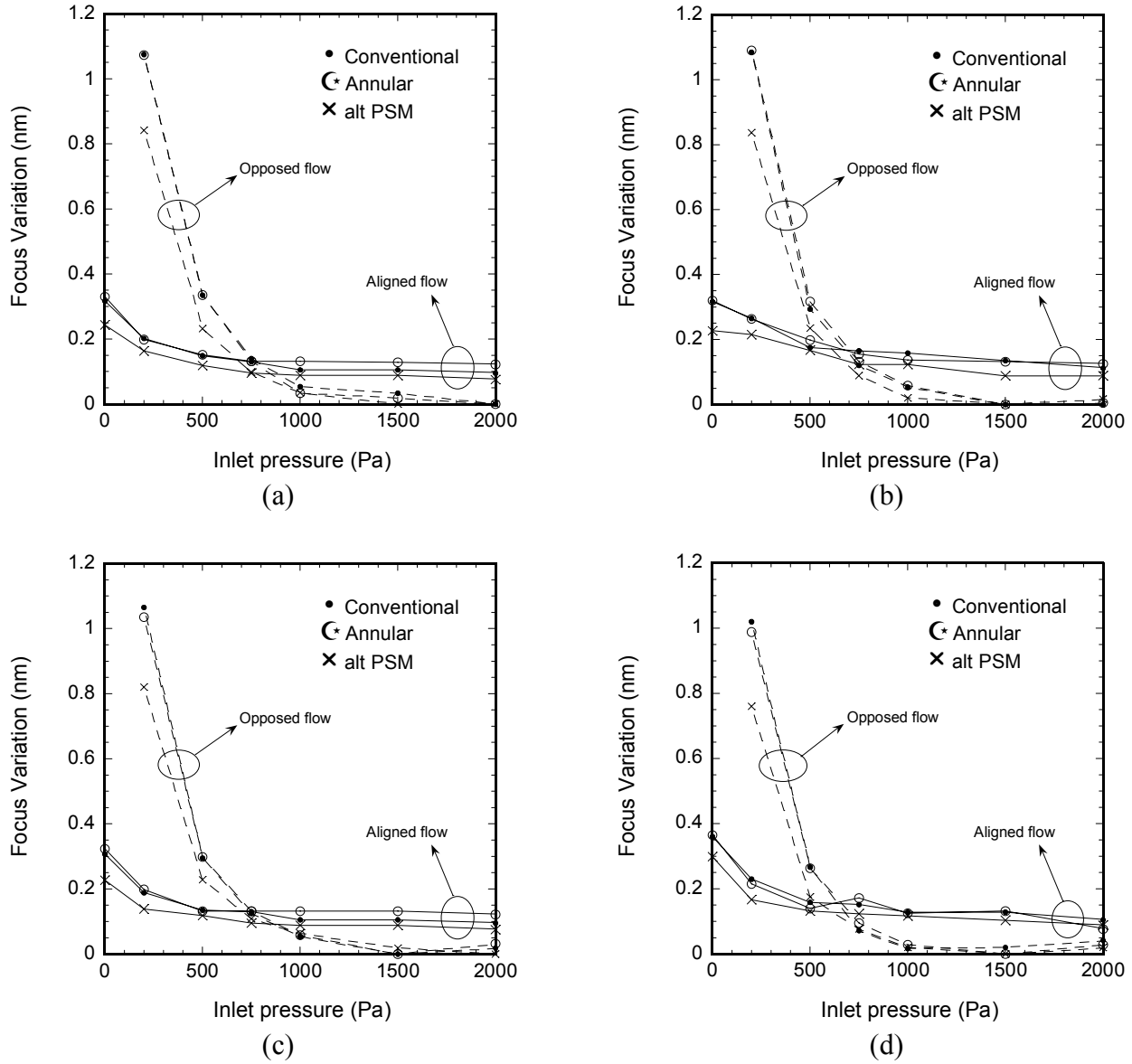


Fig. 11: Focus variation across the slit, meaning, the difference in focus shifts between the left and right sides of the exposure slit. The solid lines indicate the case of aligned fluid flow while the dashed lines represent the case of opposed fluid flow. Figs. 11(a) and 11(b) were examined at the point of 0.25 s of scanning (i.e., “transient case”), with Fig. 11(a) being the results for the 1st chip, and Fig. 11(b) being the results for the 43rd chip. Figs. 11(c) and 11(d) represent the results in the steady state scanning situation, with Fig. 11(c) being the results for the 1st and Fig. 11(d) being the results for the 43rd chip. The “1st chip” means the first scanning chip of the wafer and the 43rd chip is the “hottest chip” in the wafer during the whole exposure process, for the particular scanning/stepping simulation case examined here.

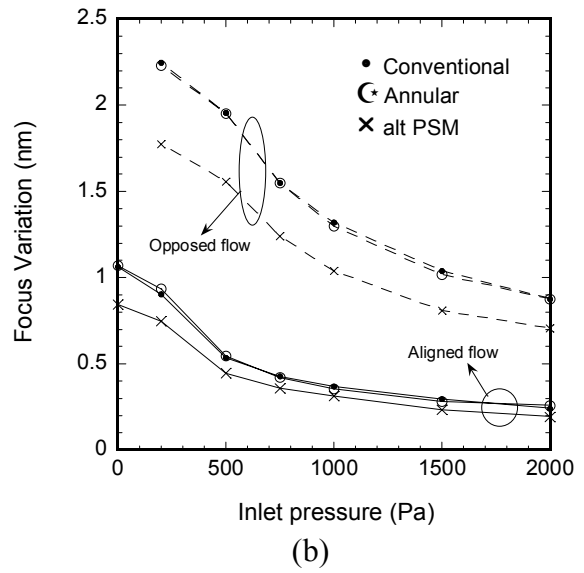
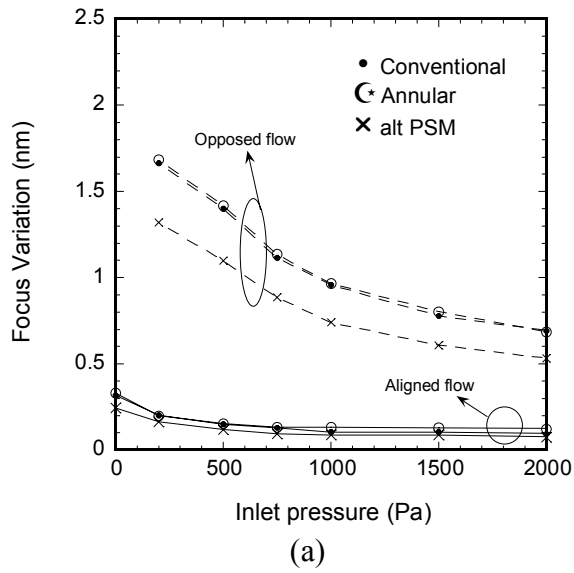


Fig. 12: Focus variation across chips under different fluid flow conditions, as computed at the center of the exposure slit. Transient exposure times were examined between the 0.01 sec and 0.25 sec scan times. Fig. 12(a) pertains to the first chip, while Fig. 12(b) pertains to the 43rd chip.

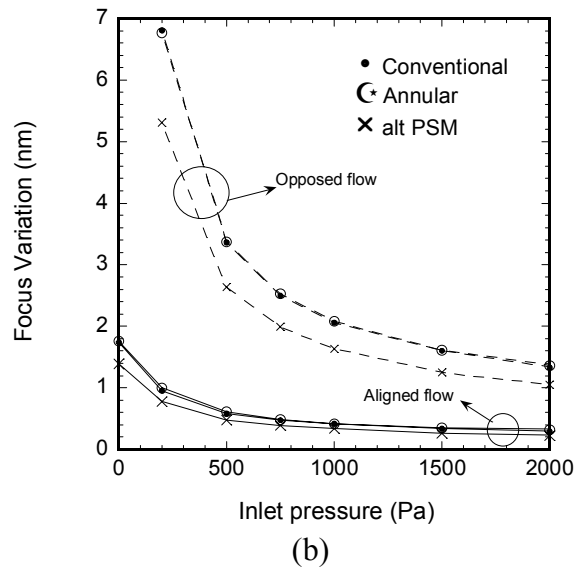
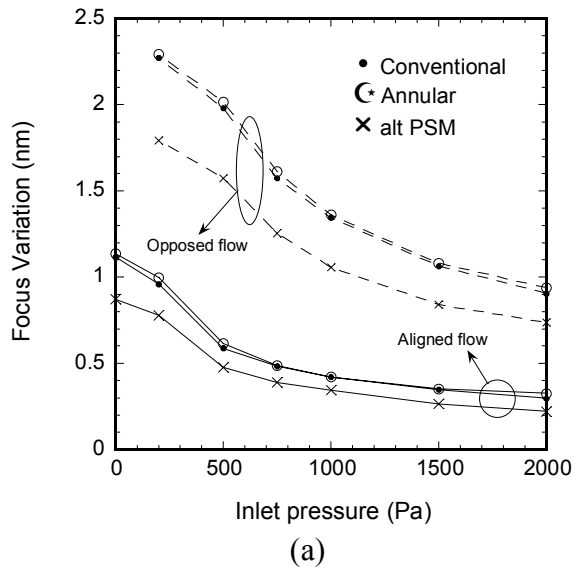


Fig. 13: Focus variation across wafer under different fluid flow conditions, as computed at the center of the exposure slit. (a) Focus variation across wafer at transient 0.25 s exposure scan time. (b) Focus variation across wafer for the “steady-state” exposure model.